Advanced Image Processing Package for FPGA-Based Re-Programmable Miniature Electronics

Vladimir I. Ovod, Christopher R. Baxter, Mark A. Massie
Nova Sensors, 320 Alisal Rd, Suite 104, Solvang, CA 93463
(805) 693-9600
vlad@novasensors.com

Paul L. McCarley
Air Force Research Laboratory, Munitions Directorate (AFRL/MNGI), Eglin AFB, FL 32542
(850) 882-3910

ABSTRACT

Nova Sensors produces miniature electronics for a variety of real-time digital video camera systems, including foveal sensors based on Nova's **V**ariable **A**cuity **S**uperpixel **I**mager (VASI™) technology. An advanced image-processing package has been designed at Nova Sensors to re-configure the FPGA-based co-processor board for numerous applications including motion detection, optical, background velocimetry and target tracking. Currently, the processing package consists of 14 processing operations that cover a broad range of point- and area-applied algorithms. Flexible FPGA designs of these operations and re-programmability of the processing board allows for easy updates of the VASI™ sensors, and for low-cost customization of VASI™ sensors taking into account specific customer requirements.

This paper describes the image processing algorithms implemented and verified in Xilinx FPGAs and provides the major technical performances with figures illustrating practical applications of the processing package.

Keywords: Foveal Sensors, Image Processor, FPGA, FPA, Variable Acuity, Superpixels, Programmable, Visible, Infrared, UAV

1. INTRODUCTION

A new class of imaging sensors, "foveal sensors", has been developed at Nova Sensors for the purpose of providing a wide field of view at high frame rates with one or more very high spatial resolution regions on areas of interest. These sensors are based on Nova's Variable Acuity Superpixel Imager (VASI™) technology [1]. The VASI™ devices provide the capability for the user or controlling processor to change the spatial configuration of high- and lower spatial resolution pixels *at the frame rate*. The multi-resolution characteristics of this sensor help to reduce the total number of effective pixel values that are multiplexed off of the focal plane array (FPA) with each frame, thereby reducing the data bandwidth required to produce an accurate representation of the salient portions of the image, while continuing to observe the total field of view (TFOV) at lower resolutions.

Designed according to principles of functioning of human vision, these new imaging sensors will enable a large new class of real-time algorithms specifically designed for autonomous target acquisition (ATA) and tracking) targets of interest. It is increasingly important to exploit the use of this class of imaging sensor with new algorithms that are specifically designed to make use of the spatially tunable nature of the FPA. To date, Nova Sensors has produced a variety of "first-cut" acquisition and tracking algorithms for the VASI™. These algorithms are being implemented into Nova Sensors' miniature image processor board that has been introduced in [2]. A brief description of the image processor is given in Section 2.

The goal of this paper is to present the advanced image-processing package for field programmable gate arrays (FPGA) based re-programmable miniature electronics (see Section 3). The basis of the processing package is VASI™ pre-processor and multiple target acquisition discussed in Section 3.1 and Section 3.2, correspondingly.

The VASI™ pre-processor includes Image Reconstruction, one and two point Non-Uniformity Correction (NUC), NUC controller, Bad Pixel Replacement (BPR), and 2-bit VASI™ FPA controller (see Figure 2). A set of 14 other processing operations that could be implemented as a parallel or sequential FPGA-Processor to support a consumer requested mission are presented in Section 3.3 and listed in Table 1. A potential candidate for further FPGA implementation is morphological target acquisition discussed in Section 4.

Table 1. Point- and area-applied algorithms included in the advanced image-processing package

Algorithms Implemented in FPGA	Master Card Sections 3.1 and Section 3.2	Parallel Processor Section 3.3
Point-applied algorithms:		
- Image reconstruction from a compressed frame	*	
- One- and two-point non-uniformity correction including the median offset computation from the masked FPA-row data	*	
- Arbitrary pixel revectoring	*	
- Bad pixel replacement	*	
- Pixel-based mean and standard deviation computation	*	
- Spectral attenuation compensation		*
- Atmospheric attenuation compensation		*
Area-applied algorithms:		
- Intensity-weighted centroid target tracking (up to four targets)	*	
- Real-time Fast Fourier Transform (FFT) and Power Spectral Density (PSD) computation		*
- Convolution processing		*
- Median and average filters		*
- Optical flow vector field computation		*
- Background velocimetry		*
- Zero Crossing Technique		*
Further FPGA implementation		
- Morphologically-based Target Acquisition		

2. MINIATURE IMAGE PROCESSOR BOARD

Figure 1 shows a photograph of the miniature image processor board set. The board set includes a number of Xilinx Virtex II FPGA devices (each part contains at least one million gates of programmable logic) to support a wide variety of processing algorithm operations and incorporates enough static RAM to support growth to image sizes of up to 2048 x 2048 pixels per frame. The processor board set is capable of receiving digital camera image data at effective total pixel rates of up to 80 megapixels/second. Depending upon the complexity of the processing function, multiple boards can be interfaced to partition the task into multiple parallel processing streams. More details regarding processor board performance have been presented in [2].
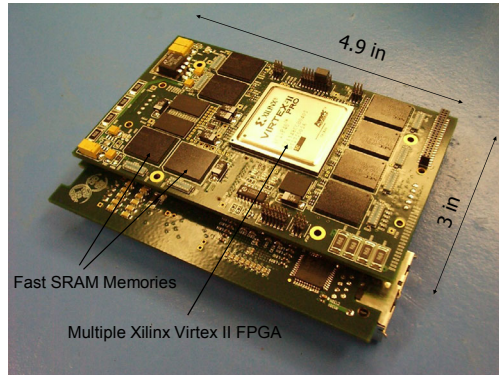
Figure 1. Nova's miniature image/signal processor board set, designed to incorporate multiple Xilinx Virtex II FPGAs and fast SRAM memories.

3. ADVANCED IMAGE PROCESSING PACKAGE

The advanced image-processing package has been designed at Nova Sensors to re-configure the FPGA-based co-processor board for numerous applications including motion detection and target tracking. Figure 2 shows that the basis of the processing package is the VASI™ Pre-Processor and Multiple Target Acquisition to be discussed in Section 3.1 and Section 3.2. A set of 14 other processing operations that could be implemented as a parallel or sequential FPGA-Processor to support a consumer requested mission are presented in Section 3.3. The architecture supports expandability. Additional parallel processor boards are shown as dashed lines. These Miniature Image Processing Cards can be added to the Master Processing Card as required.
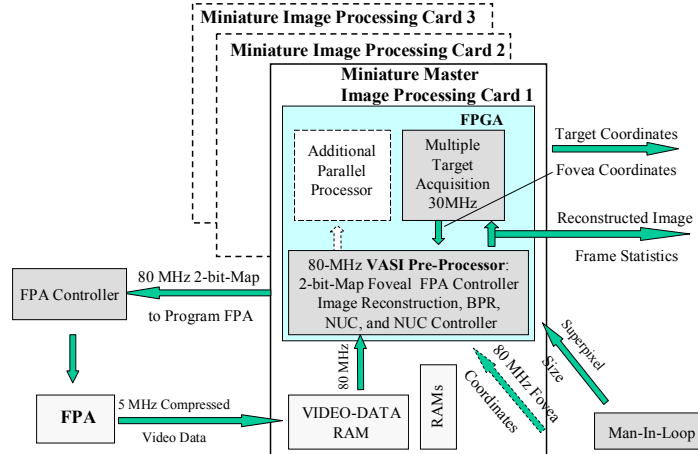

Figure 2. Re-programmable miniature foveal sensor for multiple target acquisition. Additional parallel processors are shown as dashed lines.

3.1. VASI™ PRE-PROCESSOR

3.1.1. Up"-bit and "Left"-bit Controller to program FPA
The VASI™ Pre-Processor firmware design performs the following functions on the sensor data stream: "Up"-it and "Left"-bit Controller to program the VASI™ FPA, Image Reconstruction, Bad Pixel Replacement (BPR), and Non-Uniformity Correction (NUC, see Figure 2).

"Up" and "Left" denote the connectivity between an individual pixel and its upward and leftward nearest neighbors. Each pixel is programmed into a specific "superpixel" state, and it will "know" how to share its charge with neighbors so that a resulting superpixel distribution is produced. High frame rates are possible using VASI™ technology by programming the device into a superpixel state; pixels (whether they be "standard pixels" or "superpixels") need to deliver only one analog data value per frame. This will minimize the total number of pixel values to be read off of the FPA ("compressed" images are read off FPA), thus maximizing effective frame rate. An example of "Left"- and "Up"- maps is presented in Figure 3 (see images b) and c), respectively). These maps have been used, correspondingly, to program the configuration shown in the image d. Four dark areas in Figure 3 (images b and c) correspond to the four foveae. Their coordinates and dimensions have been computed by the Multiple Target Acquisition function of the master image-processing card (Figure 2). In the given example the image size is 128x128 pixels while the superpixel size is 16x16 pixels.

3.1.2. Image Reconstruction

As it has been shown above the VASI™ technology allows for "compressing" images (decreasing the number of pixel values) read from the FPA while maintaining full resolution surrounding areas of interest, and retaining detection capability over the entire field-of-view (FOV). To "uncompress" images, an Image Reconstruction function is performed in the VASI™ Pre-Processor. Figure 3 shows both a full resolution image (image a) and one that has been reconstructed (image d) by the VASI™ Pre-Processor after the FPA has been programmed into a superpixel configuration with two foveal regions. Both figures contain a point-target and a resolved target. The full resolution image on the left was generated by the CHAMP infrared scene generation program [3], [4], and contains 16384 pixel values (128x128). The size of the full resolution frame has been reduced from 16384 pixel values to 718 pixel values in the "compressed" superpixellated image on the right. Each superpixel is 16x16 in size. This superpixel configuration with two foveal regions produces 23 times less pixel values per frame than the full resolution image. For each frame, the Image Reconstruction function computes the standard deviation and mean values of the image that could be used for further processing.
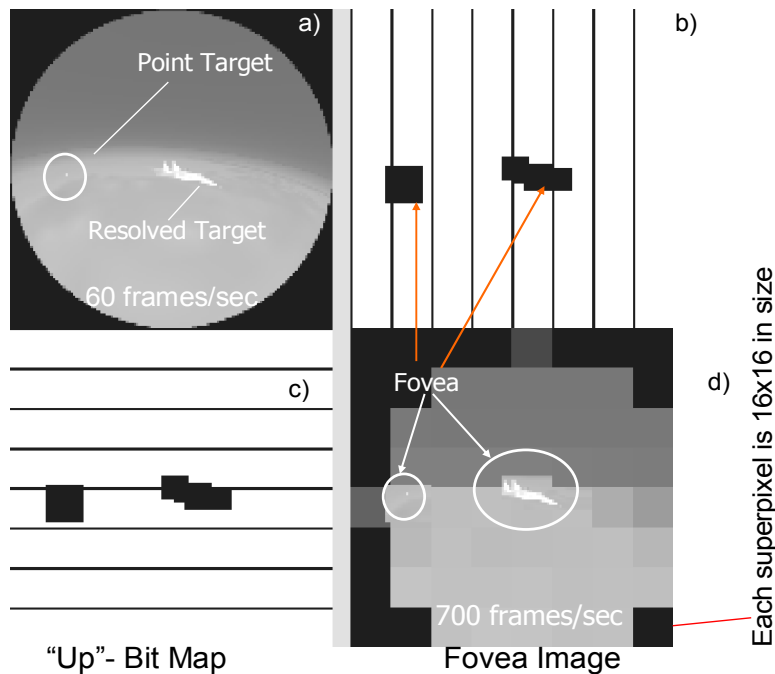

Figure 3. Comparison of the full resolution image a) and foveal image d). Both figures contain a point-target and a resolved target image. The size of the full resolution frame is 128x128 pixels. The superpixel size in the right figure is 16x16 pixels. The b) and c) images represent the "Left" and "Up" bits, respectively, used to program the configuration shown in the image d).

3.1.3. Two Point Spatial Non-Uniformity Correction (NUC), Bad Pixel Replacement (BPR), NUC Controller, and Arbitrary Pixel Revectoring

Fixed pattern spatial non-uniformities in the CMOS fabrication process used to fabricate readout integrated circuits (ROIC) cause variations in the gain and offset characteristics of amplifiers within individual ROIC unit cells or columns (see Figure 4.a). To fix this problem (see Figure 4.b), the spatial "two-point" non-uniformity correction is included in the VASI™ Pre-Processor, i.e.

$$s_{ij} = G_{ij}^1 x_{ij} + C_{ij}^1 \quad for \ i = 1, \ n_x \ and \ j = 1, \ n_y \tag{1}$$

where x_{ij} and s_{ij} are the image values before and after the spatial NUC is applied. Coefficients G_{ij}^1 and C_{ij}^1 are gain and offset respectively that fix the spatial non-uniformities and n_x and n_y are the total number of pixels along the corresponding axis, X and Y (see also Figure 7).

Two-point NUC is typically performed so that, assuming the linear behavior of all pixels over a specified flux range, all pixels will exhibit the same signal swing response. If a few columns in FPA sensors are protected from illumination, the offset C_{ij}^1 can be computed in the FPGA as means and averages from the above-mentioned corresponding columns. As a result of high temporal noise, low responsivity, etc., some pixels can be classified as "bad" pixels. The VASI™ Pre-Processor automatically replaces these pixels with values of "good" spatial neighbors such that a "nice-looking picture" is produced by the FPA. The NUC Controller applies corrections to pixel values within high resolution (i.e. fovea) areas only. In order to keep the effective frame rate of a large pixel-count imager high, FPAs typically multiplex parallel channels of data at the output. If such an FPA is used, the VASI™ Pre-Processor "shuffles" the parallel channels of data together to re-assemble a properly displayed image. The so-called Arbitrary Pixel Revectoring (APR) provides arbitrary spatial re-mapping of these pixel values by accessing re-vector address memory that stores the appropriate re-vectored locations.

Figure 4. Full resolution infrared image before NUC and BPR (the left figure), and the corresponding image after the spatial NUC and BPR (the right figure).

3.2. AUTONOMOUS MULTIPLE TARGET ACQUSITION (ATA)

An Autonomous Multiple Target Acquisition technique for foveal sensors such as VASI™ has also been developed. The current FPGA implementation of this technique allows for acquiring up to four targets simultaneously. Figure 3 (images c, b, and d) illustrates a specific example when four foveae have been allocated by the ATA algorithm around a relatively large image of a resolved target and a single point target. Nova's Multiple Target Acquisition technique does not use thresholds to detect targets of interest, but instead uses an area- and intensity- computation technique. Using this technique, the size of each rectangular fovea depends on the shape and dimension of the image area selected as a most competitive target candidate (see Figure 5 and Figure 6). The left frame in Figure 5 shows a full resolution image. When the ATA algorithm is applied, the FPA is configured into a superpixel mode with three fovea located over detected objects. This can be seen in the reconstructed image on the right.
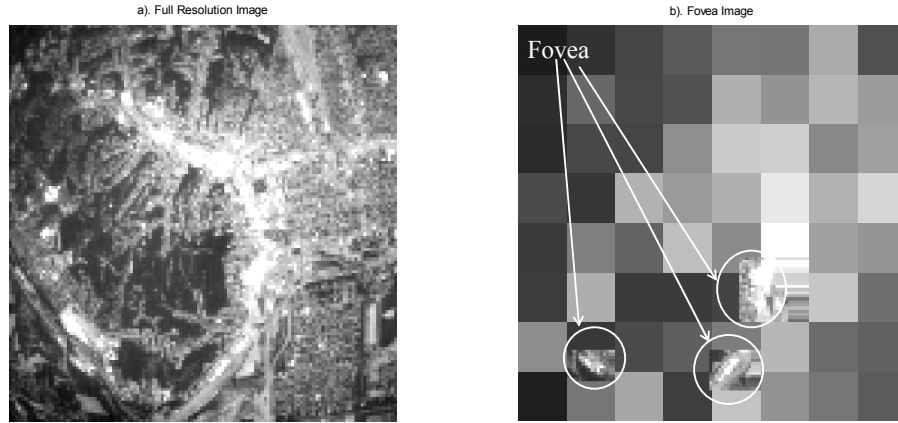
Figure 5. Comparison of a full resolution image (left figure) and foveae image (right figure). The size of the full resolution frame is 128x128 pixels. The superpixel size in the right image is 16x16 pixels. The size of image on the right is about 23 times smaller than the full resolution image on the left. The corresponding "Up" and "Left" bits Maps are shown in Figure 6.
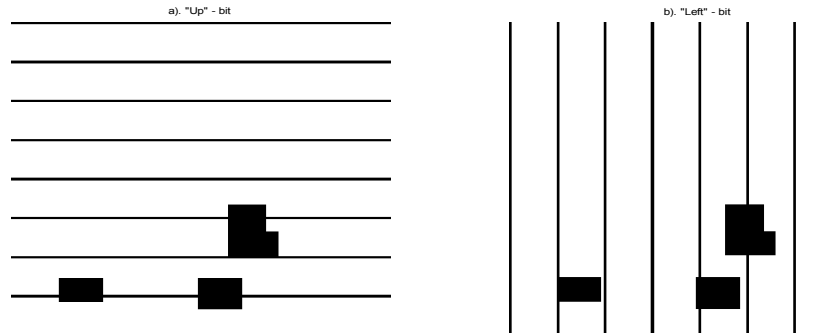

Figure 6. The left and right images above represent the "Up" and "Left" bits, respectively, used to program the FPA configuration shown in Figure 5.b. The FPA format is 128x128 pixels. The superpixel size is 16x16 pixels. Three dark areas correspond to the three fovea whose coordinates and dimension have been computed by the VASI™ Pre-Processor (see Figure 2).

3.3. ADDITIONAL PARALLEL PROCESSOR

A list of point- and area-applied algorithms implemented in the Image Processor's FPGA is presented in Table 1. The second column of the table indicates algorithms implemented in the Master Card (see Figure 2). Additional parallel processors (shown in Figure 2) could include the rest of the point-applied and area-applied algorithms listed in the third column in Table 1. The well-known convolution operations as well as median and averaging filters implemented in an FPGA are not discussed in this paper.

3.3.1. Atmospheric and Spectral Attenuation Correction

Figure 7 shows the combined spatial non-uniform, and spectral- and atmospheric attenuation corrections implemented in Xilinx FPGA under the Low Earth-Orbiting Imaging Sensor (LEOIS) program (sponsored by AFRL/VSSS). Spatial two-point NUC (see Eq. (1)) has been discussed in Section 3.1.2. Signal variations due to the selective absorption of radiant energy, $\gamma_{i\,j}$, as a function of wavelength across the spectral range of the hyperspectral sensor may be compensated using one-point spectral correction:

$$s_{i\,j}^{s} = G_{i\,j}^{s}\, s_{i\,j} \quad , \quad for\ i = 1,\, n_x \ \ and\ \ j = 1,\, n_y \tag{2}$$

where pre-computed gain corrections, $G_{i\,j}^{s}$, are stored in SRAM.

$$G_{ij}^s = \frac{1}{\gamma_{ij}}, \ \ for \ i = 1, \ n_x \ \ and \ \ j = 1, \ n_y \tag{3}$$

They are clocked out of memory and applied synchronously with the pixel data stream. Atmospheric NUC compensates the atmospheric attenuation by the one-point correction

$$s_{ij}^a = G_{ij}^a s_{ij}^s \ \ , \ \ for \ i = 1, \ n_x \ \ and \ \ j = 1, \ n_y \tag{4}$$

where atmospheric attenuation gain, $G^a{}_{ij}$, is computed by

$$G_{ij}^a = \frac{1}{\tau_i}, \ \ for \ i = 1, \ n_x \ \ and \ \ j = 1, \ n_y \tag{5}$$

and 'τ_i' is the atmospheric transmittance shown in Figure 8 for the middle- (MWIR, the left figure) and the long- (LWIR, the right figure) infrared wavelength bandwidths.

In the IP FPGA hardware developed at Nova, separate address ranges in memory are programmed with atmospheric attenuation gain data, $G^a{}_{ij}$, and spectral correction gains, $G^s{}_{ij}$.

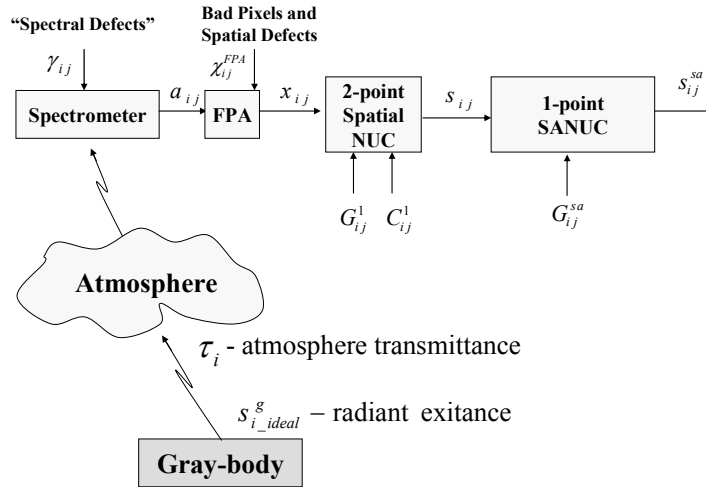## Spatial, Spectral, and Atmospheric Correction

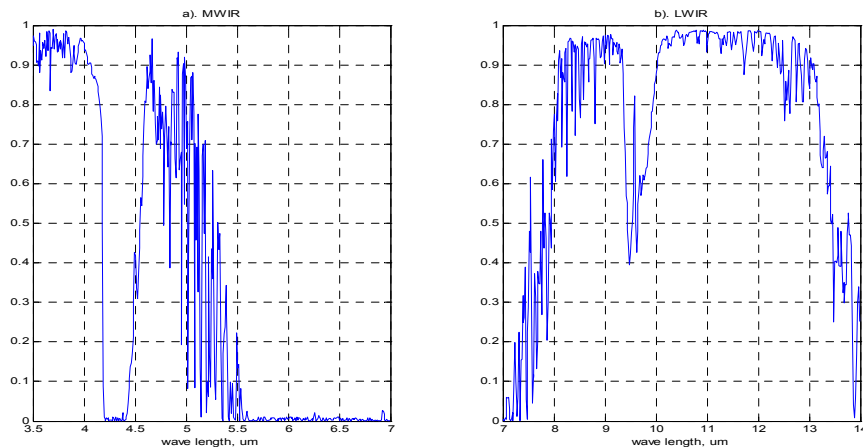**Figure 7**. Spatial, spectral and atmospheric corrections.

Figure 8. Atmosphere transmittance in MWIR (the left figure) and in LWIR (the right figure) measured for a dry atmosphere from Earth to Space.

3.3.2. Real-time Pixel-Based FFT and PSD Computation for Target Acquisition

256- and 1024-point Fast Fourier Transform (FFT) modules have been designed by Nova Sensors using fixed-point arithmetic. The FFT design has been implemented in the Xilinx Virtex II family of field programmable gate arrays. This FFT module computes real-time power spectra on the VASI™ camera data stream.

Figure 9 illustrates one of the practical FFT-module applications in the "hyper-temporal" processing algorithm set for evaluation of temporal signatures of objects that emit modulated IR energy in the audio regime. In such an application, the FFT module performs real-time evaluations of power spectral densities (PSDs) for each pixel in the imager, followed by conditional tests to attempt "to find" single-pixel objects with such temporal signatures. More details regarding the FFT module design and its implementation for "hyper-temporal" processing have been published in [5].
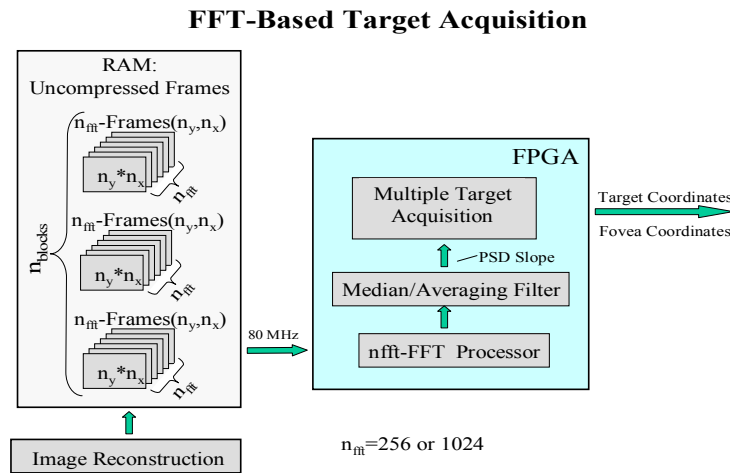
FFT-Based Target Acquisition

Figure 9. Simplified block diagram of the FFT-based Target Acquisition. Nova's Virtex II-based PSD processor permits dynamically-adjustable parameters to be set: n_{blocks} is the number of the coadded FFT transforms; $\{n_y*n_x\}$ is the frame size; n_{fft} is the number of FFT points, i.e. 256 or 1024.

3.3.3. Optical Flow Vector Field Computation
Other applications exist that require a real-time estimation of the image velocity flow field (see Figure 10). This may be applied to sensor egomotion sensing, object identification and tracking against a moving background.
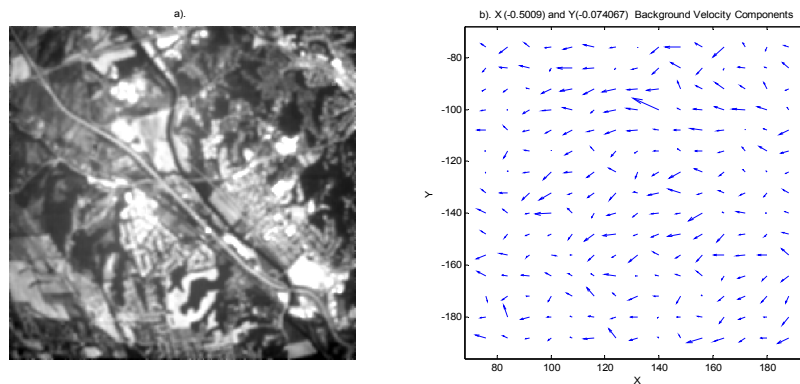

Figure 10. Background velocimetry using Optical Flow: The original IR image shown in the left frame indicates motion of the sensor from left to right. The Optical flow field shown in the right figure estimated the background velocity of {-0.5 and 0.074} in X- Y-directions, respectively, in relative numbers.

In addition, these techniques can be used to compute focus of expansion, time to contact and many other motion properties of images that can be used to control robots or other moving platforms. Tracking systems can use the extracted velocity information, while segmentation of moving objects can be performed by using the detection of motion discontinuities [6]. Using optical flow fields, spatial clutter may be reduced by eliminating pixel responses moving in specified directions. A "first-cut" Virtex II design for an optical flow computation engine based on principals developed by Horn and Schunk [7] has been designed. An example of an application of optical flow for background velocity measurement is shown in Figure 10. The original IR image shown in the left figure indicates motion of a space-based IR sensor from West to East. The optical flow field shown in the right figure estimated the background velocity of {-0.5 and 0.074, relative numbers} in X- Y-directions, correspondingly. It shows that the optical flow technique confirms that the sensor moves from left to right.

3.3.4. Background Velocimetry

We have developed an alternative technique for background velocimetry based on the computation of time- and spatial- derivatives for each of four bars A-, B-, C, and D- arranged along the corresponding borders of an FPA image (see Figure 11). This technique may use Nova's VASI™ sensors to keep frame rates high, but it may also be applied in general to common image frame sequences. An example of the background velocity measurement is shown in Figure 12.
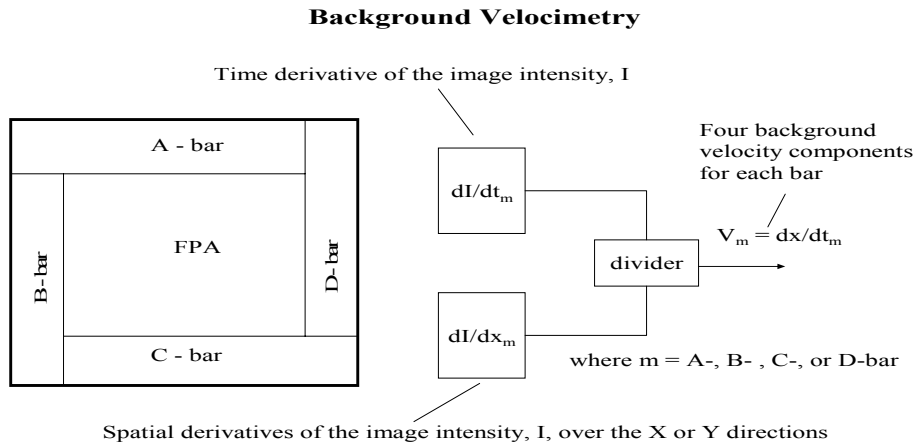

Figure 11. Background velocimetry: time- and spatial derivatives are computed for each of four bars A-, B-, C, and D- bars allocated virtually along the corresponding borders of FPA.
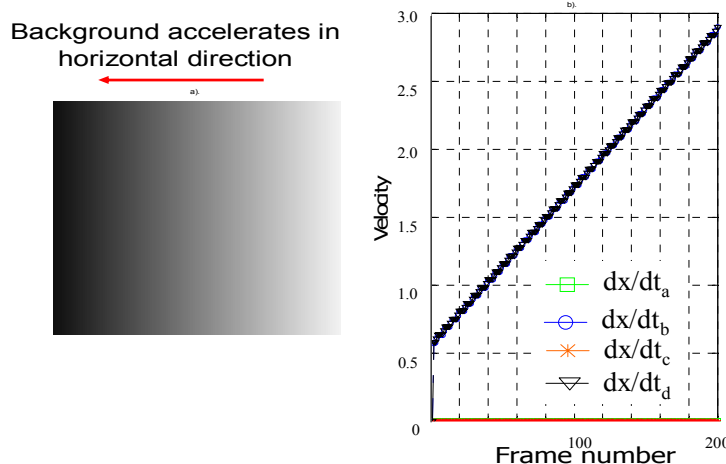

Figure 12. The background-motion sensor response (the right figure) from the non-periodic background accelerated in horizontal direction (the left figure).

The background-motion sensor response is presented in the right figure for the non-periodic background accelerated in horizontal direction in the left figure. Zero velocities measured at the A- and C-bars (marked by squares and stars, respectively) confirm the background motion along the X-axis. The linear sensor response at B- and D- bars (see the left figure, lines B and D, marked by circles and triangular, respectively) is in agreement with linear acceleration of the background.

3.3.4. Zero Crossing Technique

Zero Crossing Technique (ZCT) includes three major processing steps: blurring of each frame, computing Difference-of-Gaussian (DoG), and zero crossing (extracting pixels with intensities close to zero at the DoG output). ZCT can be used for edge detection and as a preprocessing step for Differential Velocity Detection developed at Nova Sensors, as a stay-along target tracker, and as a preprocessing operation for a more sophisticated target tracker operating in the midst of cluttered background. The use of the Zero Crossing Technique for target acquisition is demonstrated in Figure 13. The left figure is the original image that contains a point-target and an air-target image. The right image is the ZCT's output.
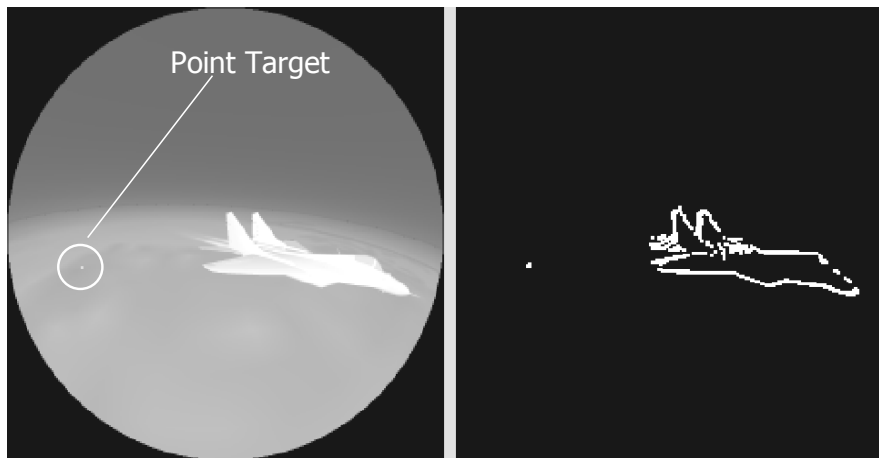

Figure 13. Use of Zero Crossing Technique for target acquisition and for edge detection. The left figure is the original image that contains a point-target and an air-target image [3], [4]. The right image is the ZCT's output.

4. FURTHER FPGA IMPLEMENTATION: MORPHOLOGICALLY-BASED TARGET ACQUISITION

Our further work includes implementation of Morphologically-based Target Acquisition (MTA) techniques into FPGA implementations. MTA is based on morphological operations, i.,e., dilation, erosion, opening, and closing [9],[10]. Figure 14 illustrates a block diagram of MTA developed at Nova Sensors using an adaptive computation of the threshold by Renyi's entropy [11]. Figure 15 demonstrates competitive target-acquisition performances. The left figure shows an IR image with a cluttered background moving from the left to the right (see also Figure 10), and a synthetically inserted point-target moving from the top to the bottom. The right figure is the accumulative output from the Morphological Filter that rejects the cluttered background and acquires the point-target. The right figure plots the point-target trajectory during a set of frames. No false alarms were computed.

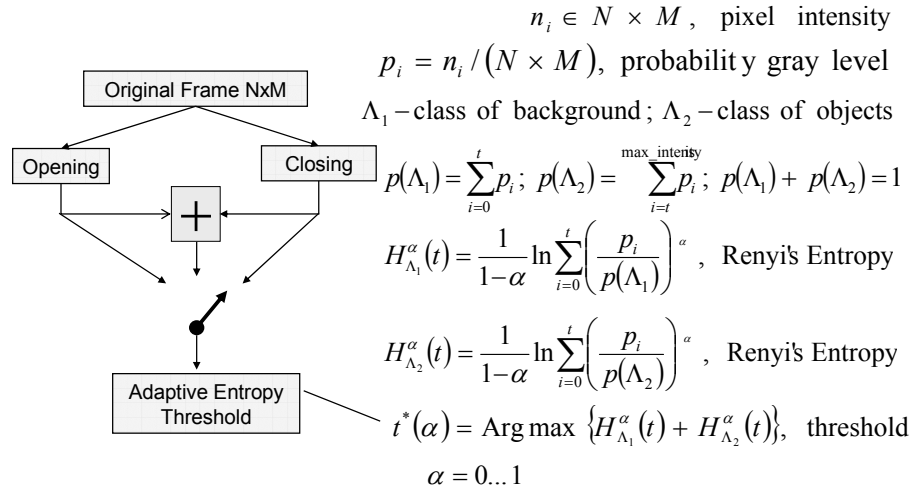# Adaptive Morphologically-Based Target Acquisition:
Renyi's Entropy Threshold

$$n_i \in N \times M, \quad \text{pixel intensity}$$

$$p_i = n_i / (N \times M), \quad \text{probability gray level}$$

$$\Lambda_1 - \text{class of background}; \quad \Lambda_2 - \text{class of objects}$$

$$p(\Lambda_1) = \sum_{i=0}^{t} p_i; \quad p(\Lambda_2) = \sum_{i=t}^{max\_intensity} p_i; \quad p(\Lambda_1) + p(\Lambda_2) = 1$$

$$H_{\Lambda_1}^{\alpha}(t) = \frac{1}{1-\alpha} \ln \sum_{i=0}^{t} \left(\frac{p_i}{p(\Lambda_1)} \right)^{\alpha}, \quad \text{Renyi's Entropy}$$

$$H_{\Lambda_2}^{\alpha}(t) = \frac{1}{1-\alpha} \ln \sum_{i=0}^{t} \left(\frac{p_i}{p(\Lambda_2)} \right)^{\alpha}, \quad \text{Renyi's Entropy}$$

$$t^*(\alpha) = \text{Arg max} \left\{ H_{\Lambda_1}^{\alpha}(t) + H_{\Lambda_2}^{\alpha}(t) \right\}, \quad \text{threshold}$$

$$\alpha = 0...1$$

[Block diagram: Original Frame NxM → Opening / Closing → + → Adaptive Entropy Threshold]

Figure 14. Block diagram of Morphological Target Acquisition (MTA) with adaptive computation of threshold using Renyi's entropy.
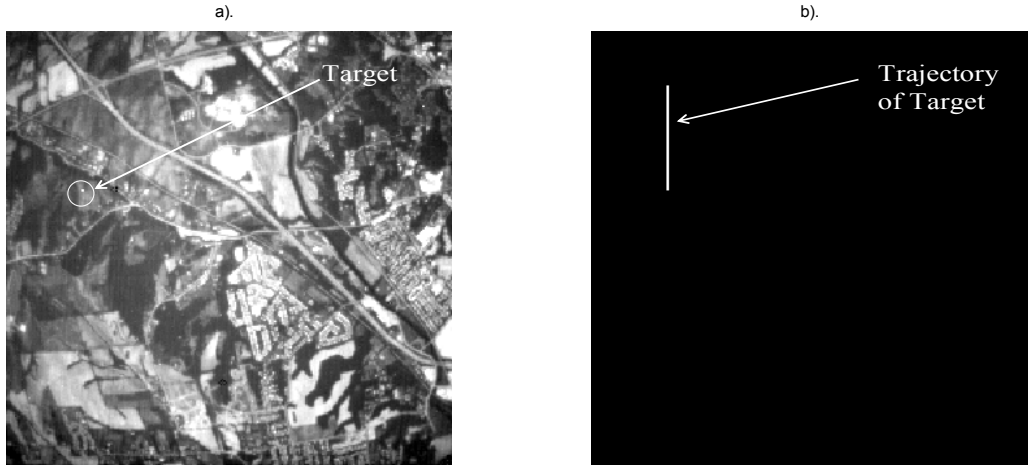

Figure 15. The left figure illustrates an IR image with a cluttered background moving from right to left (see also Figure 10) and with a point-target moving from the top to bottom. The right figure is the accumulative output from the Morphological Filter that rejects the cluttered background and acquires the point-target.

5. CONCLUSIONS

All of the image-processing algorithms listed in Table 1 have been developed for VASI™ sensors and have been implemented in the miniature FPGA-based processing board (see Figure 1) developed by Nova Sensors. The major performances of the each technique as well as examples of their practical applications were discussed in Section 2 and Section 3. Flexible FPGA designs of these techniques and re-programmability of the processing board allows for low-cost and quick turn-around of customized applications of VASI™ and other state of the art imaging sensors, taking into account specific customer requirements.

6. ACKNOWLEDGEMENTS

7. ABBREVIATIONS

ATA - autonomous target acquisition
ATT - autonomous tracking targets of interest
BPR - bad pixel replacement
FFT - Fast Fourier Transform
FPGA - Field Programmable Gate Arrays
NUC - non-uniformity correction
PSD - Power Spectral Density
TFOV - total field of view
VASI™ - Variable Acuity Superpixel Imager (Nova Sensor's Trade Mark)
ZCT – zero crossing technique

8. REFERENCES

[1]. P. L. McCarley, Mark A. Massie, and J. P. Curzan, "Large format variable spatial acuity superpixel imaging: visible and infrared systems applications". SPIE Proc., Infrared Technology and Applications XXX, vol. 5406, pp. 361-369, Orlando, 2004.

[2]. C. R. Baxter, T. R. Cicchi, M. A. Massie, and P. McCarley, "Miniature embedded real-time image processor system for smart sensor systems". SPIE Proc., Infrared Technology and Applications XXX, vol. 5406, pp. 743-754, Orlando, 2004.

[3]. D. L. Garbo, E. M. Olson, D. R. Crow, C. F. Coker and D. A. Cunard, "IR model development for a high-speed imaging fuze", SPIE Proc., Infrared Technology and Applications XXIV, Orlando, 1998.

[4]. D. L. Garbo, E. M. Olson, D. R. Crow, C. F. Coker, and D. A. Cunard, "Low-altitude IR terrain and sea model development for a high-speed imaging fuze". SPIE Proc., Technologies for Synthetic Environments: Hardware-in-the-Loop Testing IV, vol. 3697, pp. 340-350. 1999.

[5]. J. Kristl, M. A. Massie, V. I. Ovod, J. P. Curzan, and C. R. Baxter. "Hyper temporal detection of boost phase missiles using VASI Sensing and HTI algorithms", MD-SEA Conference, Monterey Naval Postgraduate School, Paper E5, November 20, 2003.

[6]. M. Swati and R. Etienne-Cummings, "A 2-D Normal Optical Flow Chip". IEEE ISCAS 2003, Bangkok, Thailand.

[7]. B.K. Horn and B.G. Schunk, "Determining Optical Flow". Artificial Intelligence, vol. 17, pp. 185 – 203, 1981.

[8]. J. T. Caulfield, V. Ovod, R. Coussa, C. Baxter, and M. Massie, "Advanced on FPA and near FPA image processing for IRFPAs", SPIE Proc., Infrared Technology and Applications XXXI, vol. 5783, Orlando, 2005.

[9]. C. Andraud, J. Lafait, A. Beghdadi, and J. Peiro, "Entropy applied to morphological analysis and modelisation of nanomaterial optical properties". J Phys. III F, France 7, pp. 549-557 March 1997.

[10]. N. Dong, G. Jin, Bo Qi, and J. Ma, "New approach to detect dim moving point targets based on motion analysis". SPIE Proc., Signal and Data Processing of Small Targets, vol. 4473, pp. 34-42, 2001.

[11]. P. Shoo, C. Wilkins, and J. Yeager. "Threshold selection using Renyi's entropy", Pattern Recognition, vol. 30, No. 1, pp. 71-84, 1997.